Nanoscale

Accepted Manuscript

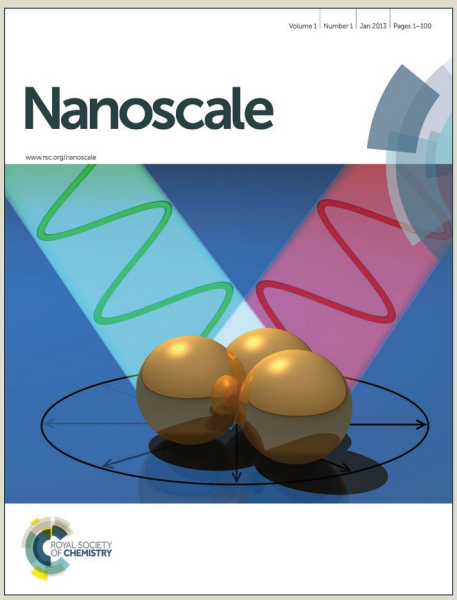

ROYAL SOCIETY OF CHEMISTRY

www.rsc.org/nanoscale

Journal Name

ARTICLE TYPE

Cite this: DOI: 10.1039/xxxxxxxxxx

Supracolloidal helices from soft Janus particles by tuning particle softness†

Qing-Zhi Zou,[a] Zhan-Wei Li,*[a] Zhong-Yuan Lu,[b] and Zhao-Yan Sun*[a]

Received Date
Accepted Date

DOI: 10.1039/xxxxxxxxxx

www.rsc.org/journalname

Because of the unique architectures and promising potential applications of biomimetic helical structures in biotechnology and nanotechnology, the design and fabrication of these structures by experimentally realizable anisotropic colloidal particles remain one of the most challenging tasks in materials science. Here we show how soft Janus particles self-assemble into supracolloidal helices with distinctive structural characteristics, including single helices, double helices, and Bernal spirals, by properly tuning particle softness. We further examine the kinetic mechanisms governing the formation of different helical structures by using particle-based dynamics simulations. Our results provide a new way for experimentally fabricating structure-controllable supracolloidal helices solely from the self-assembly of soft Janus particles.

1 Introduction

Helical architectures are abundant in nature and ubiquitous in living systems, which have diverse potential applications in the fields such as optics, optoelectronics, sensors, and catalysis [1–4]. Designing and fabricating biomimetic helical superstructures through the self-assembly of colloidal particles are becoming more and more important and challenging tasks in materials science. Anisotropic colloidal particles, which have been proven to be appropriate building blocks for the fabrication of various helical superstructures, have attracted a lot of attention in recent years [5–7]. A number of helical structures have been experimentally realized from the self-assembly of shape-anisotropic particles such as magnetite nanocubes [5], Au nanorods [6], and magnetic dumbbells [7]. Meanwhile, patchy particles with surface anisotropy emerge as a new class of building blocks for self-assembly of well-controlled supracolloidal helices [8,9]. For example, a Bernal spiral [10] described as a stack of face-sharing tetrahedra, alternatively named as Boerdijk-Coxeter helix [11], has been assembled from patchy colloids with three pairs of patches and antipatches [8]. Similarly, a vast collection of biomolecular mimetic supracolloidal helices have been achieved by the self-assembly of patchy particles with controlled arrangements and interactions of patches [9]. However, patterning a colloidal particle's surface in such a sophisticated and well-controlled geometry may not be immediately accessible by present experimental techniques [12,13]. Therefore, the design and fabrication of biomimetic helical superstructures by simple and experimentally realizable surface-anisotropic colloidal particles remain a major scientific and technological challenge.

As the simplest case of patchy particles [14,15], Janus particles exhibit remarkable ability to self-assemble into a large variety of highly ordered supracolloidal structures [12,13,15–19]. Especially, Bernal spirals have been experimentally realized using hard Janus particles at high salt concentration [16], and also theoretically designed through the self-assembly of Janus-type building blocks [20]. In addition, single helices and double helices were achieved via the self-assembly of soft Janus particles with deformable and anisotropic characteristics, by properly tuning Janus balance and the strength of attraction between attractive patches [21]. In experiments, soft Janus particles have been realized as Janus micelles [15,22–24], Janus microgels [25,26], Janus dendrimers [27–31], and Janus hyperbranched polymers [32]. The softness and deformability of these soft Janus particles can be quantitatively described by the elastic modulus [21,33,34], and tuned by varying the cross-linking density [35,36], the grafting density [26], the number of primary branches, the density of radical branches [28], and so on. As suggested in Refs. [16,20], the critical design rule to construct Bernal spirals is that the range of anisotropic interactions between Janus particles must be short relative to particle size. Thus, Bernal spirals were not observed in the self-assembly of soft Janus particles, due to their relatively longer-range anisotropic attraction. However, as demonstrated in Ref. [21], the range of anisotropic attraction of soft Janus particles can be well tuned by altering particle softness. Therefore, the particle softness may play an unexpectedly important role in designing various helical structures by the self-assembly of soft Janus particles.

[a]State Key Laboratory of Polymer Physics and Chemistry, Changchun Institute of Applied Chemistry, Chinese Academy of Sciences, Changchun 130022, China. E-mail: zwli@ciac.ac.cn; zysun@ciac.ac.cn
[b]State Key Laboratory of Supramolecular Structure and Materials, Institute of Theoretical Chemistry, Jilin University, Changchun 130023, China

† Electronic Supplementary Information (ESI) available. See DOI: 10.1039/b000000x/

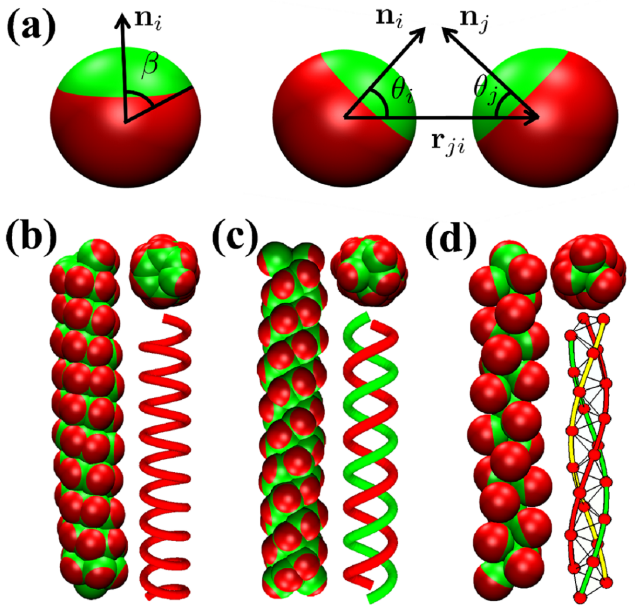

Fig. 1 Biomimetic supracolloidal helices self-assembled from soft Janus particles. (a) Graphical representation of soft Janus particle model. (b) Single helices. (c) Double helices. (d) Bernal spirals. In (b)-(d), the left part shows side view of the supracolloidal helices, and the top and bottom images in the right part show top view of the supracolloidal helices and the geometrical representation of the supracolloidal helices, respectively. The side and top views of these three types of helical structures are all extracted from simulated equilibrium structures.

Herein, we introduce a new concept in constructing helical architectures through the self-assembly of soft Janus particles with tunable particle softness. The role of particle softness is explored in self-assembling different desired helical structures with the aid of soft Janus particle model [Fig. 1(a)]. For Janus particles whose deformability is higher, the number of nearest neighbors per Janus particle is not limited to six. Thus, single helices [Fig. 1(b)] and double helices [Fig. 1(c)] can be obtained. With decreasing softness of Janus particles (i.e., Janus particles become harder), the range of anisotropic attraction becomes shorter, and the number of nearest neighbors per particle will not exceed six. Thereby, Bernal spirals [Fig. 1(d)] are obtained through the self-assembly of these Janus particles. The building blocks in our model are sufficiently simple, and the experimental implementation of soft Janus particles with tunable softness is within the reach of today's experimental capabilities[15,23,24,26,28,35–37]. Therefore, soft Janus particles with tunable softness hold significant promise for the design and fabrication of biomimetic helical superstructures.

2 Model and simulation details

Model. The soft Janus particle model (SJPM)[21,33,34] as illustrated in Fig. 1(a) is used to investigate the self-assembly of soft Janus particles. In SJPM, the soft and anisotropic attractive potential between Janus particles is expressed as

$$U_{ij} = \begin{cases} \frac{\alpha_{ij}^R}{2}\left(1-\frac{r_{ij}}{r_c}\right)^2 - f^\nu \frac{\alpha_{ij}^A}{2}\left(\frac{r_{ij}}{r_c}-\frac{r_{ij}^2}{r_c^2}\right) & r_{ij} \le r_c \equiv 1.0 \\ 0 & r_{ij} > r_c, \end{cases} \quad (1)$$

where

$$f = \begin{cases} \cos\frac{\pi\theta_i}{2\beta}\cos\frac{\pi\theta_j}{2\beta} & \text{if } \cos\theta_i \ge \cos\beta \text{ and } \cos\theta_j \ge \cos\beta \\ 0 & \text{otherwise.} \end{cases}$$

For simplicity, we use the interaction cutoff radius (r_c) as the unit of length, k_BT as the unit of energy, and choose the moment of inertia (I) and the mass (m) of the particle as the units, thus the time unit $\tau = \sqrt{mr_c^2/k_BT}$. All of the simulation parameters in this work are given in reduced units.

As illustrated in Fig. 1(a), the green part of surface represents the attractive patch and the red part represents the repulsive patch, and the directions of the attractive patches on particle i and j are specified by unit vectors $\mathbf{n}_i$ and $\mathbf{n}_j$, respectively. θ_i is the angle between $\mathbf{n}_i$ and the interparticle vector $\mathbf{r}_{ji} = \mathbf{r}_j - \mathbf{r}_i$, and θ_j is the angle between $\mathbf{n}_j$ and $\mathbf{r}_{ij} = -\mathbf{r}_{ji}$. The size of the attractive patch is described by Janus balance β, and the fraction of surface covered by the attractive patch, χ, is related to β by the relation $\chi = \sin^2(\frac{\beta}{2})$ [38,39]. The anisotropic function f ensures that the patch-to-patch alignment of soft Janus particles is energetically favorable. In Eq. 1, the magnitude of α_{ij}^R controls the strength of repulsion, α_{ij}^A controls the strength of attraction between the attractive patches, and ν controls the angular width of the attraction. Thus, both α_{ij}^A and ν control the flexibility of Janus particle aggregates. As shown in Fig. S1, the distance dependence of the anisotropic attractive potential U_{ij} presents relatively strong repulsion at short range and weak attraction at long range. With the increase of α_{ij}^R, the strength of repulsion becomes stronger, and the range of attraction becomes shorter.

As demonstrated in Refs.[21,33,34], this SJPM can be directly mapped onto experimental systems in different conditions. The parameter α_{ij}^R is related to the linear elastic modulus E of the particle by $\alpha_{ij}^R = \pi E d_{eff}^2/6$[40,41]. Here, d_{eff} is the effective diameter of soft Janus particle, and can be estimated by $d_{eff} = (\alpha_{ij}^R + \alpha_{ij}^A/2)/(\alpha_{ij}^R + \alpha_{ij}^A)$. If δ is defined as the range of attraction related to the effective diameter d_{eff}, and $(1+\delta)d_{eff} = r_c$, then δ is also related to α_{ij}^R and α_{ij}^A by $\delta = \alpha_{ij}^A/(2\alpha_{ij}^R + \alpha_{ij}^A)$. The energy minimum of the attractive potential at $r_{ij} = d_{eff}$ gives the adhesion energy $G = -U_{ij}^{min} = \alpha_{ij}^A(1-d_{eff})/4$, which determines the association strength between Janus particles and can be tuned by altering the salt concentration, pH, or temperature in experiments[21,33,34,40,42,43]. Thus, the simulation parameters α_{ij}^R and α_{ij}^A can be fixed from experimentally measurable particle properties including the elastic modulus E, the effective diameter d_{eff}, and the adhesion energy G.

Simulation details. We perform dynamic simulations in NVT condition (the number of particles, the volume, and the temperature are constant) in a $40\times40\times40$ cubic box with periodic boundary conditions. The temperature is controlled at target value by using the weak coupling Berendsen thermostat[21,33,34,44]. Although the Berendsen thermostat is unable to generate a well defined ensemble (especially for small systems), it has been widely used in simulations because the approximation yields roughly correct results for most calculated properties for large systems on the order of hundreds or thousands of atoms/molecules/particles, non-physical phenomena are rarely observed as a result of the

artefact[33,34,44–47]. The Nosé-Hoover thermostat is also used to examine the effect of the Berendsen thermostat. In this study, the effect of different thermostats on the self-assembled structures is negligible. The coarse-grained solvent particles are explicitly considered in the simulations, and for a system of N particles ($N = \rho V$), the number of Janus particles is $N_{solute} = N \times \phi$, and the number of spherical solvent particles is $N_{solvent} = N \times (1-\phi)$ (ϕ is the concentration of Janus particles in solution). The solute-solvent and solvent-solvent interactions follow the first term of Eq. (1). It should be noted that the coarse-grained model may lead to the reduction in degrees of freedom of solvent particles, and therefore, result in different entropies. But this problem may be partially solved by constructing effective coarse-grained potential which is designed to reproduce correct structure and thermodynamic properties of a given system at specific condition[21,34,40,41,48–50]. A time step $\delta t = 0.002\tau$ is used to integrate Newtonian equations of motion. All the simulations are performed with the aid of GALAMOST software package[51].

As shown in Fig. S2, for increasing values of $\alpha_{ij}^R = 396$, 1596, 9996, and 39996 in the repulsive potential $U_{ij} = \frac{\alpha_{ij}^R}{2}\left(1-\frac{r_{ij}}{r_c}\right)^2$, all the relations between the pressure and the number density can be fitted well by a parabola function ($p = \rho k_B T + \kappa \alpha_{ij}^R \rho^2$ ($\kappa = 0.101 \pm 0.001$))[48,52]. Thus, the isotropic solvent particles interacting via $U_{ij} = \frac{\alpha_{ij}^R}{2}\left(1-\frac{r_{ij}}{r_c}\right)^2$ are used to fit the equations of state. In this way, we can calibrate the parameter α_{ij}^R in different systems to reflect that the systems are effectively in constant pressure condition. In order to clarify the effect of particle softness on the self-assembly of Janus particles, we keep the pressure at a constant value by varying ρ for different values of α_{ij}^R. The values of ρ are calculated according to the obtained parabola fitting function. In the simulations, we choose $\rho = 3.0$, 1.1, 1.0, and 0.9 for the increasing values of $\alpha_{ij}^R = 396$, 1596, 9996, and 39996, respectively, to keep the pressure in different systems equal to that of the system with $\alpha_{ij}^R = 396$.

3 Results and discussion

3.1 The role of particle softness in the self-assembly of different helical structures

As demonstrated in Refs.[21,33,34], the simulation parameters α_{ij}^R and α_{ij}^A in SJPM can be fixed from experimentally measurable particle properties including the elastic modulus E, the effective diameter d_{eff}, and the adhesion energy G. In this work, we choose a series of values of α_{ij}^R to describe soft Janus particles with different softness. The corresponding relation between the chosen simulation parameters α_{ij}^R and the elastic modulus E is given in Table 1. For $\alpha_{ij}^R = 396$, 1596, 9996, and 39996, the values of the elastic modulus E are about 0.033 Mpa, 0.116 MPa, 0.667 MPa, and 2.590 MPa, respectively. Thus, with the increase of α_{ij}^R, Janus particles become harder, and the range of anisotropic attraction δ becomes shorter, as shown in Table 1 and Fig. S1. The choices of α_{ij}^R ensure that all the Janus particles in our simulations are soft and compressible as compared to conventional hard-sphere particles, which normally have a modulus about 2.0 GPa[40].

For the softest Janus particles in this work ($\alpha_{ij}^R = 396$, i.e., $E = 0.033$ Mpa), we have systematically examined the effects of Janus balance β and the strength of attraction between attractive patches α_{ij}^A (i.e. the adhesion energy G) on the self-assembly behavior in simulations with a larger box ($40 \times 40 \times 40$) compared to our previous work with a smaller simulation box ($20 \times 20 \times 20$)[21]. We find that the obtained self-assembly diagram in the G-β space ($0.00\ k_BT < G < 25.00\ k_BT$ and $0^\circ < \beta < 180^\circ$) is exactly the same as that in our previous work[21] (data not shown). When G is too large or $0^\circ < \beta \leq 105^\circ$, only the micellar clusters are obtained. The single helices [Fig. S3(a)] can be observed at about $15.00\ k_BT \leq G \leq 22.70\ k_BT$ and $115^\circ \leq \beta \leq 135^\circ$, and the double helices [Fig. S3(b)] can be observed at about $8.25\ k_BT \leq G \leq 13.20\ k_BT$ and $115^\circ \leq \beta \leq 125^\circ$.

Table 1 The relation between simulation parameters α_{ij}^R and α_{ij}^A and the experimentally measurable properties E, d_{eff}, and G. The parameters α_{ij}^R, α_{ij}^A, and δ are given in reduced units, and the reduced unit of length r_c in the model is assumed to approximately correspond to 50 nm.

E [Pa]	d_{eff} [nm]	G [k_BT]	α_{ij}^R	α_{ij}^A	δ
3.31×10^4	45.45	2.00	396	88	0.10
1.16×10^5	47.62	2.00	1596	168	0.05
6.67×10^5	49.02	2.00	9996	408	0.02
2.59×10^6	49.50	2.00	39996	808	0.01

For the other three values of α_{ij}^R, the self-assembly diagrams plotted with Janus balance β versus adhesion energy G are also constructed to display the role of particle softness in the formation of different helical structures. For the harder Janus particles with $\alpha_{ij}^R = 39996$ ($E = 2.59$ Mpa), the range of anisotropic attraction is sufficiently small as compared with that in Refs.[16,20], and then particle clustering favors self-assembly structures with at most six nearest neighbors per particle. Self-assembly diagram and typical self-assembly structures are shown in Fig. 2. It can be seen that the self-assembly diagram of $\alpha_{ij}^R = 39996$ is quite different from that of $\alpha_{ij}^R = 396$. In the range $80^\circ \leq \beta \leq 85^\circ$ that is in good agreement with the experiment[16], the Janus particles self-assemble into Bernal spirals [Fig. 2(d)], which can be described as a stack of face-sharing tetrahedra [Fig. 1(d)]. At low β and/or G, the small clusters including tetrahedra [Fig. 2(b)] and the coexistence of tetrahedra and trigonal bipyramid (TBP) [Fig. 2(c)] can be identified, as shown in Fig. 2(a). At high β and G, we also observe an arrested state composed of spirals as reported in Refs.[8] [Fig. 2(e)]. Moreover, we find that Bernal spirals are stable in the concentration range from $\phi = 1\%$ to $\phi = 7.5\%$, as shown in Fig. S4. For $\alpha_{ij}^R = 9996$ ($E = 0.667$ MPa), the self-assembly diagram [Fig. S5(a)] is very similar to that for $\alpha_{ij}^R = 39996$ [Fig. 2(a)], and Bernal spirals [Fig. S5(c)] can also be obtained at suitable values of β and G. But for $\alpha_{ij}^R = 1596$ ($E = 0.116$ Mpa), the range of anisotropic attraction is relatively long, which results in relatively high deformability of soft Janus particles. As shown in Fig. S6(c), Bernal spirals can still be observed, but the degree of order of Bernal spirals is affected. In order to quantitatively describe the effect of α_{ij}^R on the degree of order of Bernal spirals, we calculate the helical order parameter $Q_h = \frac{1}{N_{solute}} \sum_i \left\langle \frac{1}{2}\left[3\cos^2 \frac{\pi(n_i - n_0)}{2n_0} - 1\right] \right\rangle$, where n_i is the number of nearest neighbors of Janus particle i, n_0 is the number of nearest

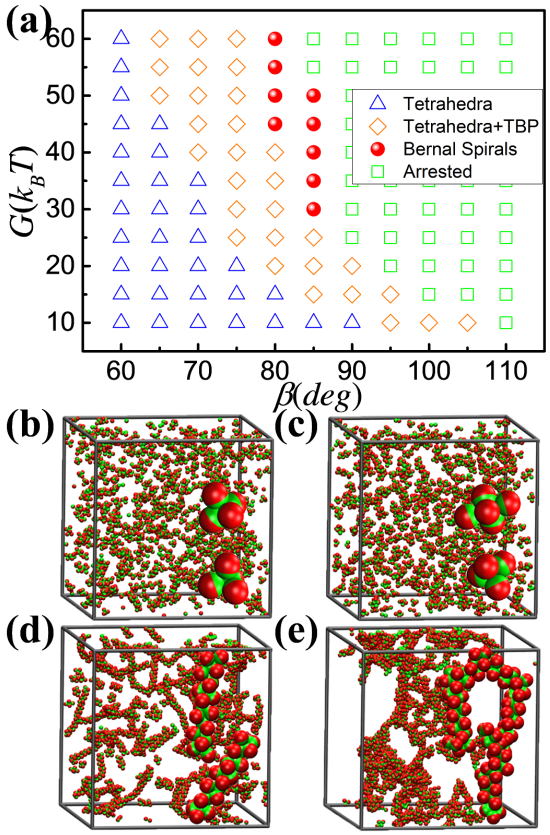

Fig. 2 (a) Self-assembly diagram of soft Janus particles in the G-β space at $\alpha_{ij}^R = 39996$ ($E = 2.59$ Mpa), $\nu = 0.25$, and $\phi = 5\%$. Blue triangles, orange diamonds, red spheres, and green squares denote the states of tetrahedra, the coexistence of tetrahedra and trigonal bipyramid (TBP), Bernal spirals, and the arrested state composed of spirals, respectively. Typical snapshots corresponding to these different states are also shown in (b)-(e).

neighbors per Janus particle in well-defined target helical structures, and N_{solute} is the total number of Janus particles in the systems. For perfect Bernal spirals, $n_0 = 6$, and $Q_h = 1.0$. As shown in Fig. S7, with increasing α_{ij}^R, Q_h becomes relatively larger. Thus, although the self-assembly diagrams are very similar and Bernal spirals can be observed for all the values of $\alpha_{ij}^R = 1596$, 9996, and 39996, the degree of order of Bernal spirals becomes higher with decreasing particle softness of Janus particles.

In order to further explore the role of particle softness in the self-assembly of different helical structures, we illustrate the center-to-center distances of nearest neighboring Janus particles for some typical self-assembled helical structures in Fig. 3, through the calculation of radial distribution function $g(r)$ in Fig. S8. As shown in Fig. 3, the average center-to-center distances of nearest-neighboring Janus particles in single helices, double helices, and Bernal spirals are 0.42, 0.47, and 0.97, respectively. Thus, in comparison with the harder Janus particles with $\alpha_{ij}^R = 39996$ ($E = 2.59$ Mpa) in Bernal spirals, the softest Janus particles with $\alpha_{ij}^R = 396$ ($E = 0.033$ Mpa) in single and double helices deform and overlap more largely with each other.

In sum, the particle softness of soft Janus particles plays an important role in the formation of different helical structures. For the softest Janus particles with $\alpha_{ij}^R = 396$, the range of anisotropic attraction is comparatively long and the particle deformability is high, single helices and double helices can be obtained by properly tuning β and G. With the increase of α_{ij}^R, Janus particles become harder, and the range of anisotropic attraction δ becomes shorter. For $\alpha_{ij}^R = 1596$, 9996, and 39996, the range of anisotropic attraction is sufficiently short to favor the formation of Bernal spirals with at most six nearest neighbors per particle as compared with that of $\alpha_{ij}^R = 396$. The degree of order of Bernal spirals becomes higher with increasing α_{ij}^R. Thus, three types of fascinating supracolloidal helices, including single helices, double helices, and Bernal spirals, can be achieved simply through the self-assembly of soft Janus particles by properly tuning particle softness.

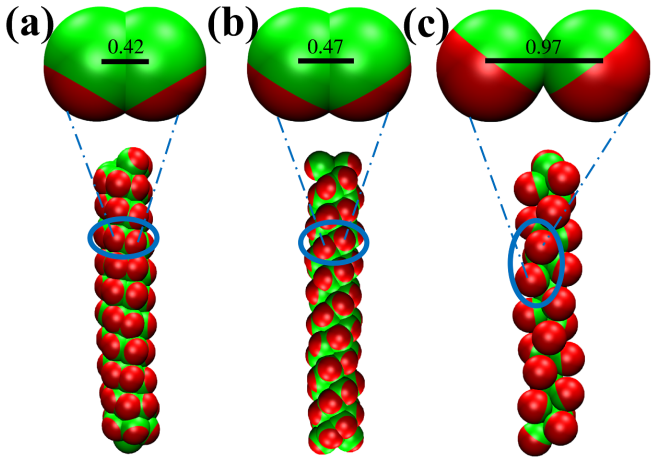

Fig. 3 The center-to-center distances of soft Janus particles in typical self-assembled helical structures. (a) Single helices at $\alpha_{ij}^R = 396$ ($E = 0.033$ Mpa), $\alpha_{ij}^A = 308$ ($G \approx 17.00\ k_BT$), and $\beta = 115°$. (b) Double helices at $\alpha_{ij}^R = 396$ ($E = 0.033$ Mpa), $\alpha_{ij}^A = 242$ ($G \approx 11.50\ k_BT$), and $\beta = 120°$. (c) Bernal spirals at $\alpha_{ij}^R = 39996$ ($E = 2.59$ Mpa), $\alpha_{ij}^A = 4420$ ($G \approx 55.00\ k_BT$), and $\beta = 80°$. The distances are given in reduced units.

3.2 Structural characteristics of different helical structures

In order to quantitatively capture the structural characteristics of different helices, we compare the distribution $S(n)$ of the number of nearest neighbors per Janus particle, n, and the distribution $P(\cos\gamma)$ of $\cos\gamma = \mathbf{n}_i \cdot \mathbf{n}_j$ for all pairs of contacting Janus particles, as shown in Fig. 4. $S(n) = N_p(n)/N_{solute}$, where the number of nearest neighbor n is calculated through counting the number of all the neighbors per Janus particle within the range of r_c, $N_p(n)$ is the number of Janus particles with the number of nearest neighbors n, and N_{solute} is the total number of Janus particles in the systems[21]. The distribution $P(\cos\gamma)$ is expected to show well-defined peaks for an ordered structure and to be flat for a completely disordered structure[18,21,38]. The face-to-face (antiparallel patches), perpendicular patches, and side-by-side (parallel patches) alignments of Janus particles can be easily characterized by the peaks at $\cos\gamma = -1.0$, 0.0, and 1.0, respectively.

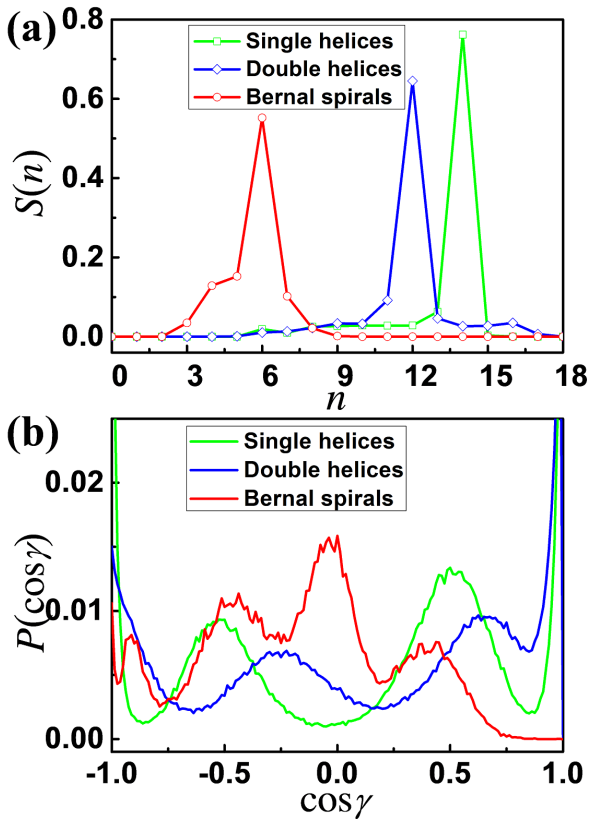

Fig. 4 Relative distributions of neighboring particles in different helical structures. (a) Distribution $S(n)$ of the number of nearest neighbors per Janus particle n. (b) Distribution $P(\cos\gamma)$ of the scalar product $(\cos\gamma = \mathbf{n}_i \cdot \mathbf{n}_j)$ for all pairs of contacting Janus particles.

As shown in Fig. 4(a) and (b), for single helices and double helices, $S(n)$ shows a narrow distribution at $n = 14$ and 12, respectively, and $P(\cos\gamma)$ shows clear double peaks at $\cos\gamma \approx -1.0$ and $\cos\gamma \approx 1.0$ and two additional peaks at special positions between $\cos\gamma = -1.0$ and $\cos\gamma = 1.0$. For Bernal spirals in Fig. 2(d), which are formed by a stack of face-sharing tetrahedra of Janus particles, $S(n)$ shows a narrow distribution at $n = 6$ since the neighbors of each Janus particle belong to a tetramer of adjacent tetrahedra with cluster size $n_s = 7$[53], and $P(\cos\gamma)$ shows four distinct peaks at around $\cos\gamma = -1.0$, -0.5–-0.33, 0, and 0.31. These four peaks originate mainly from the typical angles between the direction vectors of all pairs of contacting Janus particles in the capped trigonal bipyramid (CTBP, the basic building block of Bernal spirals[16]) with $\gamma \approx 180°$, 120°, 109.47°, 90°, and 72°, respectively. Thus, the distributions $S(n)$ and $P(\cos\gamma)$ can also be used to efficiently classify different self-assembled structures in Fig. 2, as given in Fig. S9.

3.3 Kinetic mechanism of the formation of Bernal spirals

To understand the kinetic mechanism of the formation of Bernal spirals in Fig. 2(d), we give the detailed analysis of the time dependence of the number $N_{cluster}$ of various micellar clusters with a size range of $n_s = 2$ to 7 at the initial stage of self-assembly before the growth of Bernal spirals. As shown in Fig. 5(a), the number of individual Janus particles is extremely reduced owing to the rapid formation of Janus particle dimers, and the number of Janus particle dimers also decreases rapidly with the growth of trimers and tetramers. Because clustering of harder Janus particles favors densely packed structures with at most six nearest neighbors per particle, the larger clusters with $n_s = 5$ to 7 can form, and then the number of trimers and tetramers decreases after reaching a maximum. Two types of isomers with $n_s = 6$ and 7 reported in Ref.[16] are also observed, as shown in Fig. 5(a). Therefore, our detailed analysis quantitatively verify three major steps for the formation of micellar clusters with $n_s = 2$ to 7 proposed in Ref.[16]: step-by-step addition of individual particles, fusion of smaller clusters into a larger one, and isomerization. The distribution $S(n)$ of the number of nearest neighbors per Janus particle n [Fig. 5(b)] and the typical snapshots [Fig. 5(c)-(f)] taken at different times further elucidate that the Bernal spirals with at most six nearest neighbors per particle are formed from the fusion of smaller micellar clusters in agreement with Ref.[16]. Although the structure of Bernal spirals is quite different from that of single helices and double helices, their formation mechanisms are very similar, as shown in Fig. S10 and Fig. S11.

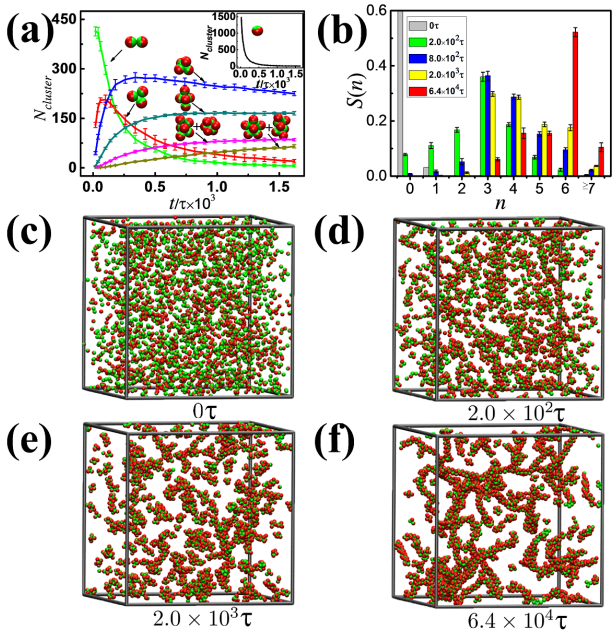

Fig. 5 Kinetics in the self-assembling process of Bernal spirals. (a) Time dependence of the number $N_{cluster}$ of various micellar clusters with a size range of $n_s = 2$ to 7 at the initial stage of self-assembly. (b) The distribution $S(n)$ of the number of nearest neighbors per Janus particle n at different times. (c)-(f) Typical snapshots taken at different times. The error bars in (a) and (b) are obtained by averaging over five different simulations.

4 Conclusions

In summary, the role of particle softness in creating different supracolloidal helices is clarified by investigating the self-assembly of a series of soft Janus particles with different degrees

of particle softness. Three types of fascinating supracolloidal helices with distinctive structural characteristics including single helices, double helices, and Bernal spirals are achieved by properly tuning particle softness. The major kinetic mechanism governing the formation of these different helical structures is the fusion of relatively unstable and smaller micellar clusters, consistent with recent experiments[16]. These soft Janus particles with tunable softness in our model are sufficiently simple, and well within the reach of today's experimental capabilities[15,23,24,26,28,35–37]. Therefore, our work paves the way for the experimental realization of a variety of biomimetic supracolloidal helices, and provides fundamental insight into the kinetic mechanism in the self-assembly of polymer colloids into biomimetic helical structures.

Acknowledgement

This work is subsidized by the National Basic Research Program of China (973 Program, 2012CB821500). The authors also appreciate the financial supports from National Science Foundation of China (21474110, 21474111, 21222407). Z.Y.L. thanks the support from Jilin Province Science and Technology Development Plan (20140519004JH).

References

1 J. K. Gansel, M. Thiel, M. S. Rill, M. Decker, K. Bade, V. Saile, G. von Freymann, S. Linden and M. Wegener, *Science*, 2009, **325**, 1513.
2 V. Percec, M. Glodde, T. K. Bera, Y. Miura, I. Shiyanovskaya, K. D. Singer, V. S. K. Balagurusamy, P. A. Heiney, I. Schnell, A. Rapp, H.-W. Spiess, S. D. Hudson and H. Duan, *Nature*, 2002, **419**, 384.
3 E. Yashima, K. Maeda, H. Iida, Y. Furusho and K. Nagai, *Chem. Rev.*, 2009, **109**, 6102.
4 T. E. Gier, X. Bu, P. Feng and G. D. Stucky, *Nature*, 1998, **395**, 154.
5 G. Singh, H. Chan, A. Baskin, E. Gelman, N. Repnin, P. Král and R. Klajn, *Science*, 2014, **345**, 1149.
6 X. Lan, X. Lu, C. Shen, Y. Ke, W. Ni and Q. Wang, *J. Am. Chem. Soc.*, 2015, **137**, 457.
7 D. Zerrouki, J. Baudry, D. Pine, P. Chaikin and J. Bibette, *Nature*, 2008, **455**, 380.
8 J. W. R. Morgan, D. Chakrabarti, N. Dorsaz and D. J. Wales, *ACS Nano*, 2013, **7**, 1246.
9 R. Guo, J. Mao, X.-M. Xie and L.-T. Yan, *Sci. Rep.*, 2014, **4**, 7021.
10 J. D. Bernal, *Proc. R. Soc. Lond. A*, 1964, **280**, 299.
11 A. H. Boerdijk, *Philips Res. Rep*, 1952, **7**, 303.
12 Q. Chen, S. C. Bae and S. Granick, *Nature*, 2011, **469**, 381.
13 F. Romano and F. Sciortino, *Nat. Commun.*, 2012, **3**, 975.
14 E. Bianchi, R. Blaak and C. N. Likos, *Phys. Chem. Chem. Phys.*, 2011, **13**, 6397.
15 A. Walther and A. H. E. Müller, *Chem. Rev.*, 2013, **113**, 5194.
16 Q. Chen, J. K. Whitmer, S. Jiang, S. C. Bae, E. Luijten and S. Granick, *Science*, 2011, **331**, 199.
17 F. Romano and F. Sciortino, *Soft Matter*, 2011, **7**, 5799.
18 F. Sciortino, A. Giacometti and G. Pastore, *Phys. Rev. Lett.*, 2009, **103**, 237801.
19 C.-L. Zhang, W. Wei, F.-X. Liang and Z.-Z. Yang, *Sci. Sin. Chim.*, 2012, **42**, 1616.
20 S. N. Fejer, D. Chakrabarti, H. Kusumaatmaja and D. J. Wales, *Nanoscale*, 2014, **6**, 9448.
21 Z.-W. Li, Z.-Y. Lu, Z.-Y. Sun and L.-J. An, *Soft Matter*, 2012, **8**, 6693.
22 A. Walther and A. H. E. Müller, *Soft Matter*, 2008, **4**, 663.
23 A. H. Gröschel, F. H. Schacher, H. Schmalz, O. V. Borisov, E. B. Zhulina, A. Walther and A. H. E. Müller, *Nat. Commun.*, 2012, **3**, 710.
24 A. H. Gröschel, A. Walther, T. I. Lobling, J. Schmelz, A. Hanisch, H. Schmalz and A. H. E. Müller, *J. Am. Chem. Soc.*, 2012, **134**, 13850.
25 D. Suzuki, S. Tsuji and H. Kawaguchi, *J. Am. Chem. Soc.*, 2007, **129**, 8088.
26 M. Bradley and J. Rowe, *Soft Matter*, 2009, **5**, 3114.
27 C. N. Likos, *Soft Matter*, 2006, **2**, 478.
28 V. Percec, D. A. Wilson, P. Leowanawat, C. J. Wilson, A. D. Hughes, M. S. Kaucher, D. A. Hammer, D. H. Levine, A. J. Kim, F. S. Bates, K. P. Davis, T. P. Lodge, M. L. Klein, R. H. DeVane, E. Aqad, B. M. Rosen, A. O. Argintaru, M. J. Sienkowska, K. Rissanen, S. Nummelin and J. Ropponen, *Science*, 2010, **328**, 1009.
29 M. Peterca, V. Percec, P. Leowanawat and A. Bertin, *J. Am. Chem. Soc.*, 2011, **133**, 20507.
30 C. Park, J. Lee and C. Kim, *Chem. Commun.*, 2011, **47**, 12042.
31 A.-M. Caminade, R. Laurent, B. Delavaux-Nicot and J.-P. Majoral, *New J. Chem.*, 2012, **36**, 217.
32 Y. Liu, C. Yu, H. Jin, B. Jiang, X. Zhu, Y. Zhou, Z. Lu and D. Yan, *J. Am. Chem. Soc.*, 2013, **135**, 4765.
33 Z.-W. Li, Z.-Y. Lu, Y.-L. Zhu, Z.-Y. Sun and L.-J. An, *RSC Adv.*, 2013, **3**, 813.
34 Z.-W. Li, Z.-Y. Lu and Z.-Y. Sun, *Soft Matter*, 2014, **10**, 5472.
35 R. Erhardt, M. Zhang, A. Böker, H. Zettl, C. Abetz, P. Frederik, G. Krausch, V. Abetz and A. H. E. Müller, *J. Am. Chem. Soc.*, 2003, **125**, 3260.
36 C. A. Angell and K. Ueno, *Nature*, 2009, **462**, 45.
37 D.-M. Lv, W. Ni, F.-X. Liang, Q. Wang, X.-Z. Qu and Z.-Z. Yang, *Chin. J. Polym. Sci.*, 2015, **33**, 1344.
38 F. Sciortino, A. Giacometti and G. Pastore, *Phys. Chem. Chem. Phys.*, 2010, **12**, 11869.
39 N. Kern and D. Frenkel, *J. Chem. Phys.*, 2003, **118**, 9882.
40 R. D. Groot and S. D. Stoyanov, *Phys. Rev. E: Stat., Nonlinear, Soft Matter Phys.*, 2008, **78**, 051403.
41 R. D. Groot and S. D. Stoyanov, *Soft Matter*, 2010, **6**, 1682.
42 D. M. Heyes and A. C. Bránka, *Soft Matter*, 2009, **5**, 2681.
43 J. K. Cho, Z. Meng, L. A. Lyon and V. Breedveld, *Soft Matter*, 2009, **5**, 3599.
44 H. J. C. Berendsen, J. P. M. Postma, W. F. Vangunsteren, A. Dinola and J. R. Haak, *J. Chem. Phys.*, 1984, **81**, 3684.
45 B. Fodi and R. Hentschke, *J. Chem. Phys.*, 2000, **112**, 6917.

46 A. Mudi and C. Chakravarty, *Mol. Phys.*, 2004, **102**, 681.
47 G. Bussi, D. Donadio and M. Parrinello, *J. Chem. Phys.*, 2007, **126**, 014101.
48 R. D. Groot and P. B. Warren, *J. Chem. Phys.*, 1997, **107**, 4423.
49 H. S. Ashbaugh, H. A. Patel, S. K. Kumar and S. Garde, *J. Chem. Phys.*, 2005, **122**, 104908.
50 S. Jain, S. Garde and S. K. Kumar, *Ind. Eng. Chem. Res.*, 2006, **45**, 5614.
51 Y.-L. Zhu, H. Liu, Z.-W. Li, H.-J. Qian, G. Milano and Z.-Y. Lu, *J. Comput. Chem.*, 2013, **34**, 2197.
52 Z.-W. Li, Z.-Y. Sun and Z.-Y. Lu, *J. Phys. Chem. B*, 2010, **114**, 2353.
53 A. I. Campbell, V. J. Anderson, J. S. van Duijneveldt and P. Bartlett, *Phys. Rev. Lett.*, 2005, **94**, 208301.